A Novel Hybrid Battery Thermal Management System for Prevention of Thermal Runaway Propagation

Sun, Z., Guo, Y., Zhang, C., Xu, H., Zhou, Q. & Wang, C.

DOI 10.1109/tte.2022.3215691
ISSN 2332-7782
ESSN 2372-2088

Publisher: IEEE

Advanced Energy Storage Technologies and Safety Management for E-Mobility

A Novel Hybrid Battery Thermal Management System for Prevention of Thermal Runaway Propagation

Zeyu Sun[a,b], Yue Guo[a], Cheng Zhang[a], Hongming Xu[b], Quan Zhou[b*], Chongming Wang[a*]

[an] *Institutes for Future Transport and Cities, Coventry University, Coventry, United Kingdom, CV1 5FB*

[b] *Department of Mechanical Engineering, University of Birmingham, Birmingham, United Kingdom, B15 2TT*

[*] Corresponding author *e-mail address*: ac8174@coventry.ac.uk (Dr Chongming Wang); q.zhou@bham.ac.uk (Dr Quan Zhou)

Abstract: Lithium-ion batteries are extensively used in electric vehicles because of their high energy density and long service life. Designing a battery thermal management system (BTMS) that prevents thermal runaway propagation in the event of abusive accidents is crucial. The goal of this study is to design a novel hybrid BTMS with both active liquid cooling and passive cooling for preventing thermal runaway propagation in the battery module. A numerical model for a battery module (16 cylindrical 18650 cells) was developed in COMSOL multi-physics software to examine the thermal runaway propagation caused by a single cell. Copper foam and expanded graphite-paraffin (EG-PCM) composite material were used for passive cooling. In addition to the thermal runaway scenario, the thermal behaviors of the battery module with the hybrid BTMS were also evaluated under the 3C discharging and driving cycle circumstances. A conventional BTMS with natural air cooling is chosen as the baseline. The findings reveal that the proposed hybrid BTMS, which uses EG-PCM with a melting temperature of 52 °C and thermal diffusivity of 9.68 mm^2/s and copper foam with a porosity of 0.7-0.9, is capable of limiting the maximum cell temperature below the thermal safety threshold (80 °C) to prevent thermal runaway propagation. Under the NEDC load cycle, the battery module can be maintained within an optimal working temperature range by passive cooling only. By applying active liquid cooling with a flow rate of 0.3 m/s for BTMS, the average temperature reduction of the battery module at a 3C discharging rate can be up to 72.5% and 52.7% compared to passive cooling with copper foam and EG-PCM, respectively. The study highlights that the combination of active liquid cooling and appropriate passive cooling is an efficient thermal management solution for Li-ion battery applications in electric vehicles, notably in the consideration of thermal safety.

Keywords: Lithium-ion battery; Thermal runaway; Copper foam; Phase change material; Graphene

Nomenclature

a_m	Mass fraction
C_{rate}	Current charge/discharge rate
$C_{p,i}$	Specific heat capacity [J/kg]
h_n	Heat transfer coefficient [W/m^2/K]
I	Current [A]
L	Latent heat [kJ/kg]
p	Pressure [Pa]
$\dot{Q}$	Heat generation rate [W]
Q_{total}	Total heat generation [J]
Q_r	Reaction heat [J]
Q_s	Side reaction heat [J]
Q_o	Ohmic heat [J]
Q_a	Active polarization heat [J]
R	Internal resistance [Ω]
T	Temperature [°C]
ΔT	Temperature difference [°C]
t	Time [s]
$\vec{v}$	Velocity [m/s]
N	Number of cells

Greek symbols

α	Thermal diffusivity [m^2/s]
ρ_i	Density [kg/m^3]
λ_i	Thermal conductivity [W/m/K]
ε	Porosity of the copper foam
μ	Dynamic viscosity [$Pa{\cdot}s$]
Φ	Diameter [mm]

Subscripts

amb	Ambient
b	Battery cell
c	Coolant
cf	Copper foam
pcm	Phase change material
s	Solid-phase
f	Filling material
Δ	Change
∇	Divergence

1. Introduction

The market for electric vehicles (EVs) is growing rapidly due to regulations driven by concerns about global warming and air pollution [1]. Lithium-ion batteries (LiBs) are widely used in EVs due to their high energy/power density and long cycle life [2]. In EVs, battery thermal management systems (BTMS) is essential to maintain their temperature in a suitable range (15-40 °C) [3]. Extreme conditions, such as mechanical, electrical, and thermal abuse, might lead to battery thermal runaway (TR) [4]. When the battery temperature exceeds 80 °C, the internal structure of the battery might be damaged and thus induce a series of exothermic side reactions. The reaction further induces a considerable amount of heat generation, forming a "heat-temperature-chain-reaction" [5]. Yuan et al. [6] studied the TR behavior of LiBs in accelerating rate calorimetry (ARC). The Peak thermal power of the high energy density LiB cell exceeded 10 kW in the thermal runaway process, causing TR propagation. Feng et al. [7] investigated the TR propagation process in a battery module. The extreme heat release rate led to the formation of a huge temperature gradient between the TR cells and neighboring cells. In worst scenarios, TR propagation might cause fire and even an explosion. Therefore, LiB thermal hazard is a grand challenge in the safety of EVs [8].

Due to issues such as low repeatability and high cost of TR experiments, numerical simulations were deployed to study the TR propagation process in the battery modules [9]. Jindal et al. [10] established a thermal abuse model for the lithium-ion battery to guide the development of BTMS. Some researchers have developed numerical models based on Ohm's Law approach to explaining the heat generation of LiBs [11][12]. Prahit et al. [13] conducted a comparative study of direct liquid cooling and indirect liquid cooling, and the established battery heat generation model only considered ohmic

heat generation and ignored reversible heat. The proportion of reversible heat in the total heat of LiBs is significantly lower than that of irreversible heat [14]. Abada et al. [15] studied the battery TR mechanism. Some abusive conditions, such as battery manufacturing defects, external extrusion, and internal short circuits during operation, cannot be precisely predicted [4]. BTMS with optimized cooling methods were adopted to prevent TR propagation [6][11]. Three cooling methods are commonly applied in BTMS such as air, active liquid, and passive phase change material (PCM) cooling [16][17]. Feng et al. [18] pointed out that BTMs only using a liquid cooling plate is insufficient to prevent the thermal runaway propagation, and they proposed that using materials with a high heat capacity or phase change material as a thermal barrier can absorb a large amount of heat and effectively enhance the effect of thermal insulation. Li et al. [19] investigated the cooling performance of BTMS with liquid cooling. Active liquid cooling improves the performance of battery modules, and a compound system was proposed to cope with different battery operation conditions. PCM as a typical cooling material has a high latent heat, which absorbs heat generated during phase transition. However, the thermal conductivity of PCM is low. Weng et al. [20] investigated the enhancement of paraffin thermal conductivity by dosing expanded graphite (EG). The PCM can be confined into the porous structure of the EG to effectively enhance the thermal conductivity of the material [21]. Metal foam is another promising material in the field of BTMS application. Saw et al. [22] developed the cooling system of the battery based on aluminum foam with porosity control. The axial thermal conductivity of the cylindrical cell is significantly higher than the radial thermal conductivity, so the temperature distribution in the axial plane is more homogeneous than that in the radial plane. In addition, the 2D model can also effectively reduce the computing time. Chen et al. [23] investigated the battery thermal

states and cycle life by coupling one-dimensional electrochemical and two-dimensional thermal models. Vadakkepatt et al. [24] proposed a numerical method to study the effect of structural porosity on the thermal conductivity of different solid phase materials. Mohammadian et al. [25] conducted a numerical simulation of the thermal behavior of a cooling fin embedded with aluminum foam. Aluminum foam as a filling material significantly enhanced the fin cooling performance. Most of the above studies were performed under normal operating conditions of LiBs or only to investigate the TR mechanism. They did not evaluate the performance of BTMS in terms of preventing TR propagation under different cooling methods. Conventionally, heat insulation is used to delay the heat transfer from the initial TR cell to surrounding cells, but this reduces the heat dissipation performance of BTMS. Rapid heat dissipation is the key to inhibiting TR propagation in the battery module.

In this study, novel methods are investigated for mitigating the challenge of preventing TR propagation through enhancing heat dissipation. We proposed a novel battery hybrid BTMS incorporating passive and active liquid cooling. A numerical COMSOL (multi-physics program) two-dimensional finite element analysis model for a battery module (16 cylindrical 18650 cells) was established to simulate the thermal runaway propagation caused by a single cell. High thermal diffusivity material (copper foam) and high latent heat material (expanded graphite-paraffin) were utilized as the passively cooling material, respectively. To comprehensively evaluate the feasibility of the hybrid thermal management solution, the thermal behaviors of the battery module were also investigated under the 3C discharging and realistic driving cycle conditions. The baseline is a conventional BTMS with natural air cooling. A comparative study was implemented to evaluate the effect of passive cooling materials and coolant flow rate on the temperature rise and temperature

uniformity of battery modules. In the following paragraphs, for simplification, liquid cooling coupled with EG-PCM as filling material is noted as 'LC-EG-PCM', and liquid cooling coupled with copper form as filling material is noted as 'LC-CF'.

The rest of this paper is organized as follows: the numerical modelling is explained in Section 2. Simulation setup and procedures are indicated in Section 3. The results and discussion are illustrated in Section 4. Finally, the conclusions of the main findings are presented in section 5.

2. Numerical modelling

Fig. 1 shows the schematic diagram of the battery module with a hybrid BTMS. Each cell is coded based on its position in the battery module. The battery module (2D dimension: 124 mm×88 mm) contains 16 cells (Samsung 18650-33G), and the internal resistance of the cells is approximately 50 mΩ [26]. The nominal specifications of the battery cell are tabulated in Table 1. The transverse and longitudinal pitches in the battery module were 20 mm and 26 mm, respectively. In the BTMS, the active cooing had a snake-shaped coolant tube (Φ: 5 mm). The space in the module was filled with either EG-PCM or copper foam. These materials are also referred to as filling materials.

To simplify the numerical simulation analysis of the BTMS, the following assumptions were made: 1) Thermal radiation was neglected and the heat generated by cells was transmitted to neighboring ones via thermal conduction and convection; 2) Heat generation of battery cells was uniform under normal operating conditions; 3) The thermophysical properties of the cooling material were regarded as being isotropic; 4) Under normal operating conditions, the heat generated by the battery was assumed to be provided only by irreversible ohmic heat, and the heat generation of reversible entropy heat is ignored.

Table 1 Nominal Specifications of Samsung 18650-33G

Item	Specification

Nominal Voltage	3.60 V
Typical Capacity	3150 mAh
Cathode	Graphite
Anode	NiCoAl (NCA)
Ethylene carbonate	LiPF6

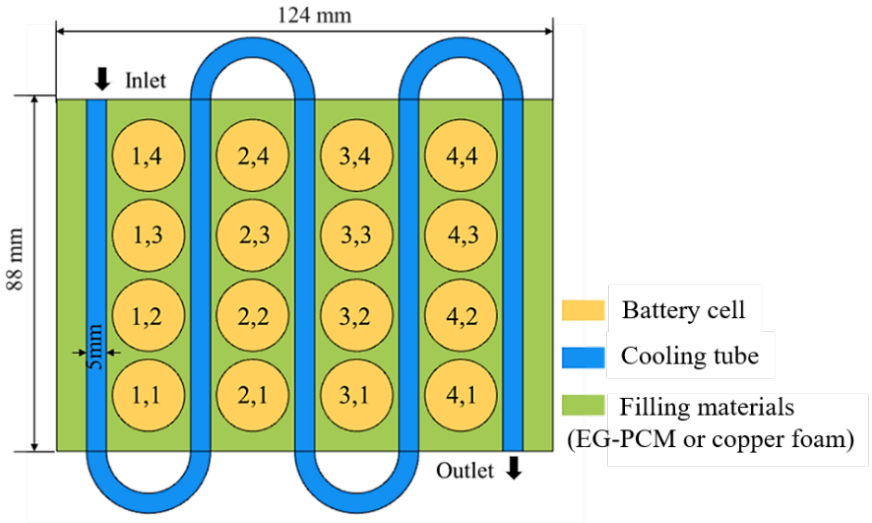

Fig. 1. Illustration of hybrid active-passive cooling BTMS.

2.1 Heat generation model

The heat generation of battery cell includes reaction heat, Q_r, side reaction heat, Q_s, ohmic heat, Q_o, and active polarization heat, Q_a. The total heat generation of battery cells, Q_{total}, can be expressed as by:

$$Q_{\text{total}}=Q_r+Q_s+Q_a+Q_o \tag{1}$$

The battery consists of multifarious constitutional materials, and it requires a complicated electrochemical model to describe the internal heat generation mechanism, which is not within the scope of this paper. A simplified way of calculating the heat generation rate of the battery is adopted in this paper. The self-heating power of the battery cell under the TR condition, which is measured by the ARC experiment in [6], is implemented in the TR propagation model to represent the heat generation rate

under TR. Although the cathode materials of the battery cells used under normal operating conditions are different from the TR case, the nominal capacity and operating voltage of selected battery cells are at the same level. The total heat generation rate of the battery module in the 3C constant current load and dynamic current load is calculated by Ohm's law:

$$\dot{Q}=N(C_{\text{rate}}I)^2R \tag{2}$$

where I denotes the current; C_{rate} denotes the current rate; R and N represent the internal resistance of the cell and the number of cells, respectively.

2.2 Thermal model

Based on the thermophysical property of materials, computational domains of the numerical model consist of several different regions, including battery, PCM, Copper foam, and liquid coolant. The energy conservation equation in the domain of the battery can be expressed as:

$$\rho_b C_{p,b}\frac{\partial T}{\partial t}=\nabla(\lambda_b\nabla T)+Q \tag{3}$$

The energy conservation equation of the copper foam domain can be expressed as:

$$(1-\varepsilon)\rho_{cf}C_{p,\,cf}\frac{\partial T_f}{\partial t}=\nabla(\lambda_{cf}\nabla T_{cf}) \tag{4}$$

Since the PCM is confined in the inter-particle space of the composite material, the convection of the melted PCM is neglected. Therefore, the momentum equation of melted PCM is not considered. The energy conservation equation of the PCM domain can be expressed as:

$$\rho_{pcm}C_{p,\,pcm}\frac{\partial T_{pcm}}{\partial t}=\nabla(\lambda_{pcm}\nabla T_{pcm}) \tag{5}$$

In the phase transition of PCM, the apparent heat capacity is calculated by the equivalent heat capacity method：

$$C_{pcm}=C_e+C_L(T) \tag{6}$$

The outer interface of filling material exchanges heat with the ambient environment by air natural convection, where the governing equation is defined as follows:

$$\lambda_f \frac{\partial T}{\partial n} = h_n (T_f - T_{amb}) \tag{7}$$

In the coolant fluid domain, coolant is considered incompressible Newtonian fluid. The momentum balance and energy conservation equation are defined as follows:

$$\rho_c C_{p,c} \frac{\partial T_c}{\partial t} + \nabla (\rho_c C_{p,c} \vec{v}) = \nabla (\lambda_c \nabla T_c) \tag{8}$$

$$\nabla \cdot \vec{v} = 0 \tag{9}$$

$$\rho_c \frac{\partial \vec{v}}{\partial t} = -\nabla p + \mu \nabla^2 \vec{v} \tag{10}$$

where ρ_i, λ_i, $C_{p,i}$, T and h_n denote density, thermal conductivity, and specific heat capacity, temperature, and heat transfer coefficient, respectively. $\vec{v}$, p and μ denote velocity, pressure, and dynamic viscosity of coolant, respectively; ε denotes the porosity of the copper foam; C_e and $C_L(T)$ denote the equivalent heat capacity of melted PCM and the latent heat distribution in phase transition interval, respectively.

3. Simulation setup

A two-dimensional thermal model was established in the Multiphysics software, COMSOL. The numerical method applied in COMSOL is based on the finite element discretization of governing equations. A direct transient solver using the PARDISO algorithm was applied to obtain the thermal transient response of the battery module through partial differential equations. The initial time step is set at 0.1 seconds to enhance the accuracy and stability of the numerical simulation. Table 2 lists the thermos-physical properties of materials in the hybrid BTMS. Two EG-PCM composite materials with different thermophysical parameters were selected, in which the thermal conductivity and melting

temperature are significantly different. The porosity of metal foam typically is 0.75-0.95 of the volume of the material [27]. Copper foam with a porosity of 0.7-0.9 was selected for numerical simulation. Table 3 lists the mass of various filling materials used in BTMS. The cell codes and their corresponding locations in the module can be found in Fig. 1. Thermal diffusivity of materials can be calculated using the following equation:

$$\alpha = \frac{\lambda}{\rho C_p} \tag{11}$$

Table 2 Thermo-physical properties of battery cell EG-PCM and copper

	Units	Battery cell [6]	EG-PCM 1 [28]	EG-PCM 2 [29]	Copper [28]
Density	kg/m^3	2800	1000	866	8920
Thermal conductivity	W/m/K	5 (Radial)	3.59	16.60	385
Heat capacity	J/kg/K	1143	1790	1980	380
Latent heat	kJ/kg	--	175	181	--
Melting temp.	°C	--	35	52	--
Transition interval temp.	°C	--	3	3	--
Thermal diffusivity	m^2/s	--	2.00E-06	9.68E-06	1.13E-04

Table 3 Mass of filling materials used in BTMS

	Units	Copper foam porosity: 0.7	Copper foam porosity: 0.9	EG-PCM 1	EG-PCM 2
Density	kg/m^3	2676	892	1000	866
Mass	kg	0.81	0.27	0.30	0.26

Using a grid independence study, appropriate cell size is chosen to balance simulation accuracy and computational time. The grid structure of the computational domain and the results of mesh independence studies are shown in Figs. 2a and 2b. The average temperature of a probe point on the battery module with coolant and without coolant was used to study mesh independence. The heat

generation rate of the single cell is set to 4W. When the grid number reaches a grid number of 10976 (maximum element size: 6.5 mm), the results converged to a steady state.

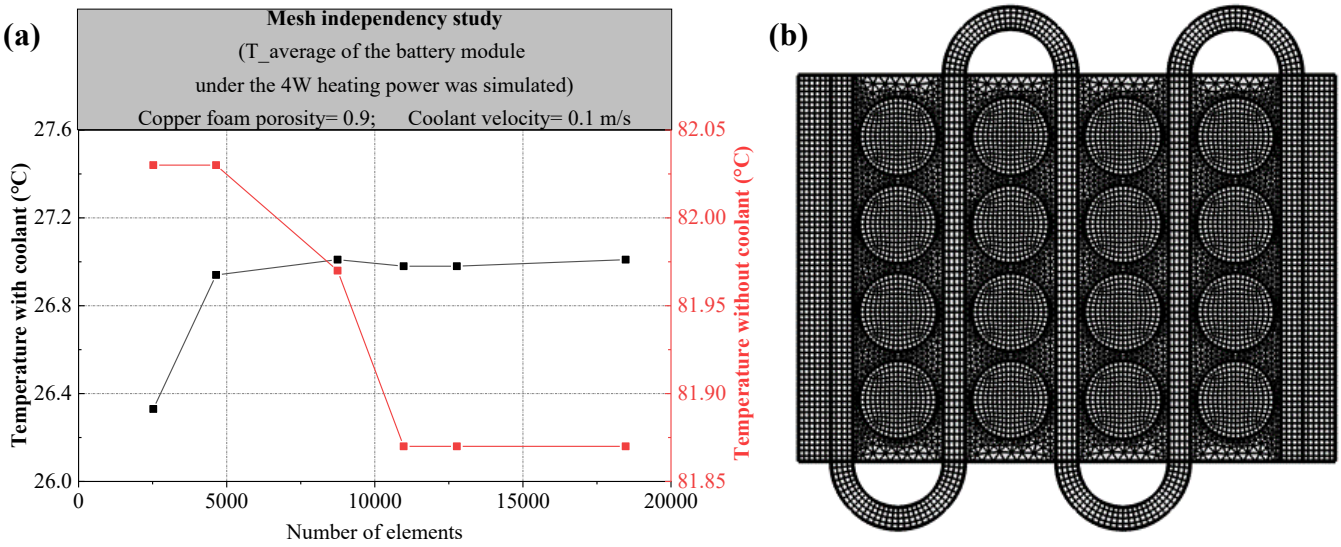

Fig. 2. Mesh independency study: (a) cell temperature; (b) selected grid structure.

Table 4 lists the initial boundary conditions. Each component of the BTMS model is considered to be in close contact in simulation. Therefore, the contact thermal resistance between interfaces can be neglected [23]. The coolant outlet pressure is set to inhibit backflow. Thermal insulation boundary condition was set to the top and bottom of BTMS. The range of air-free convection heat transfer coefficient is 2.5 to 25 W/m^2/K [30]. The environmental boundary conditions of the BTMS model are regarded as natural convection with a heat transfer coefficient of 15 W/m^2/K [31]. The inlet velocity discussed in this study, the Reynolds number is lower than 2100, and it is reasonable to set the laminar flow for the coolant. Reynolds numbers (*Re*) are generally calculated to determine the fluid dynamic flow conditions using the following equation:

$$Re=\frac{\rho \vec{v} \Phi}{\mu} \tag{12}$$

Table 4 Simulation boundary settings

Parameter	Units	Setting

Ambient temperature	℃	25
Fluid dynamic conditions	--	Laminar Flow
Liquid inlet temperature	℃	25
Liquid inlet velocity	m/s	0.01, 0.1, 0.2, 0.3
Outlet pressure	pa	0
Heat transfer coefficient	$W/m^2/K$	15

To pinpoint the highest temperature cell in the battery module, the average temperature of the battery module with hybrid active-passive BTMS and with passive BTMS only under a self-heating power of 10W were separately simulated, and the results are illustrated in the Appendix (Fig. 1A and Fig. 2A). The results indicated that the highest temperature position in the battery module with hybrid BTMS and only passive BTMS is located in Cell (4,3) and Cell (2,3), respectively. The local heat accumulation induced by the layout of the battery module resulted in the non-uniformity temperature distribution. Cell (4,3) with the highest temperature is designated as the one that experienced TR. Fig. 3 shows the heat release rate of Cell (4,3) during TR. This heat release rate curve is extracted from [6] where the heat generation rate of a Samsung 18650-33G cell under TR is measured by the ARC test. Based on simulation results, apart from Cell (4,3), Cell (4,2) and Cell (1,4) consistently show the maximum and minimum temperatures, respectively. Apart from the above TR simulation, cells working under normal conditions, including an aggressive 3C constant current discharge/charge and a mild dynamic driving cycle, were simulated to assess the hybrid active-passive cooling BTMS. Fig. 4 shows the current load of the cell under the New European Driving Cycle (NEDC) selected in this study. The duration and distance of a single driving cycle are 1180 s and 11 km, respectively.

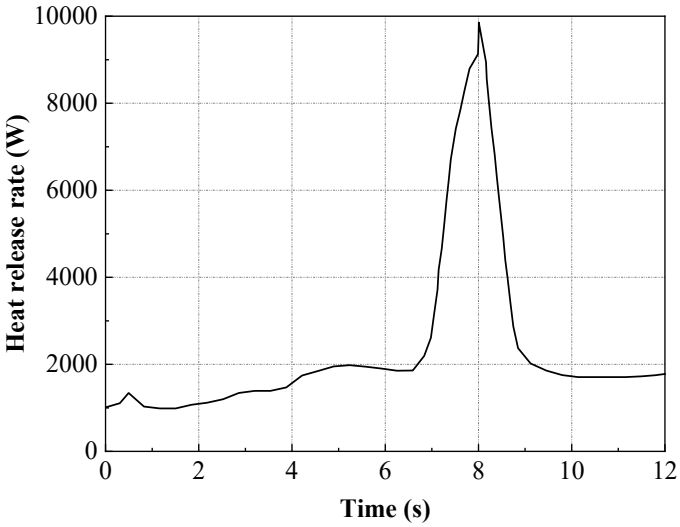

Fig. 3. The heat release rate of TR cell (ARC data extracted from [6]).

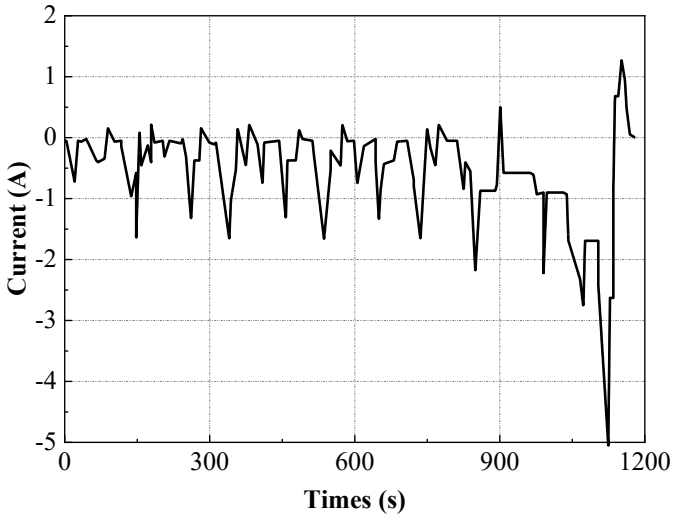

Fig. 4. Current load of the cell under NEDC (data extracted from [32]).

Model validation was performed to ensure the accuracy of the numerical model. Fig. 5 shows the comparison of the simulation results with the experimental data. The experimental data comes from the experimental study on the temperature evolution of battery modules with PCM cooling reported by Sabbah et al. [28] The experimental data and predicted results showed good agreement, indicating that the study can employ the numerical methods mentioned above.

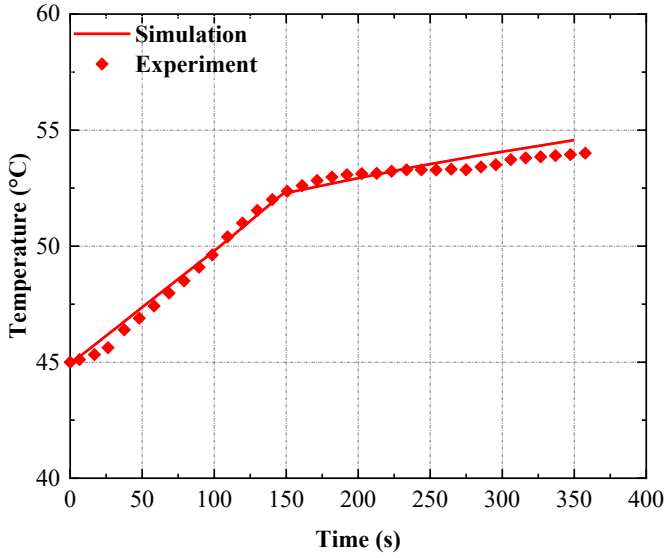

Fig. 5. Comparison between simulation results with the experimental data from literature [28]

4. Results and Discussion

This section includes three parts. The first section mainly focused on the performance of the novel hybrid BTMS in preventing the TR of a single cell from spreading to adjacent cells. The second and third parts are for the assessment of the BTMS in maintaining the battery module within a proper temperature window during normal operating conditions.

4.1 Prevention of TR propagation

The average cell temperature of three selected batteries during the single-cell TR event is depicted in Fig. 5. The simulation was conducted at a temperature of 25 °C and an active liquid cooling flow rate of 0.3 m/s. Those selected cells are the TR cell (Cell (4, 3)) as well as the cells with the highest (Cell (4, 2)) and the lowest (Cell (1, 4)) temperatures in the module. Two categories of filling materials were utilized in the module, including copper foam with porosities of 0.7 and 0.9, and EG-PCM composites with thermal conductivities of 3.59 W/m/K and 16.60 W/m/K. The filling materials functioned as heat sinks/heat dissipation enhancers. The decomposition of SEI of the battery cell is from 80 °C to 120 °C [4]. Accordingly, a threshold temperature of 80 ℃ is highlighted in plots by a dashed line, representing a critical limit for battery thermal stability. Furthermore, the propagation of thermal runaway in a battery module with natural air cooling was simulated, and the results are included in Appendix Fig. 3A.

The results indicate that the copper foam is effective in achieving this goal, especially with a lower porosity of 0.7. More specifically, Cell (4,2) reached a maximum temperature of 48.9 °C and 60.7 °C for copper foam with porosities of 0.7 and 0.9, respectively. In comparison to EG-PCM 2, EG-PCM 1 with low thermal conductivity was unable to effectively inhibit the spread of thermal runaway, demonstrating that increasing thermal conductivity is critical for PCM performance.

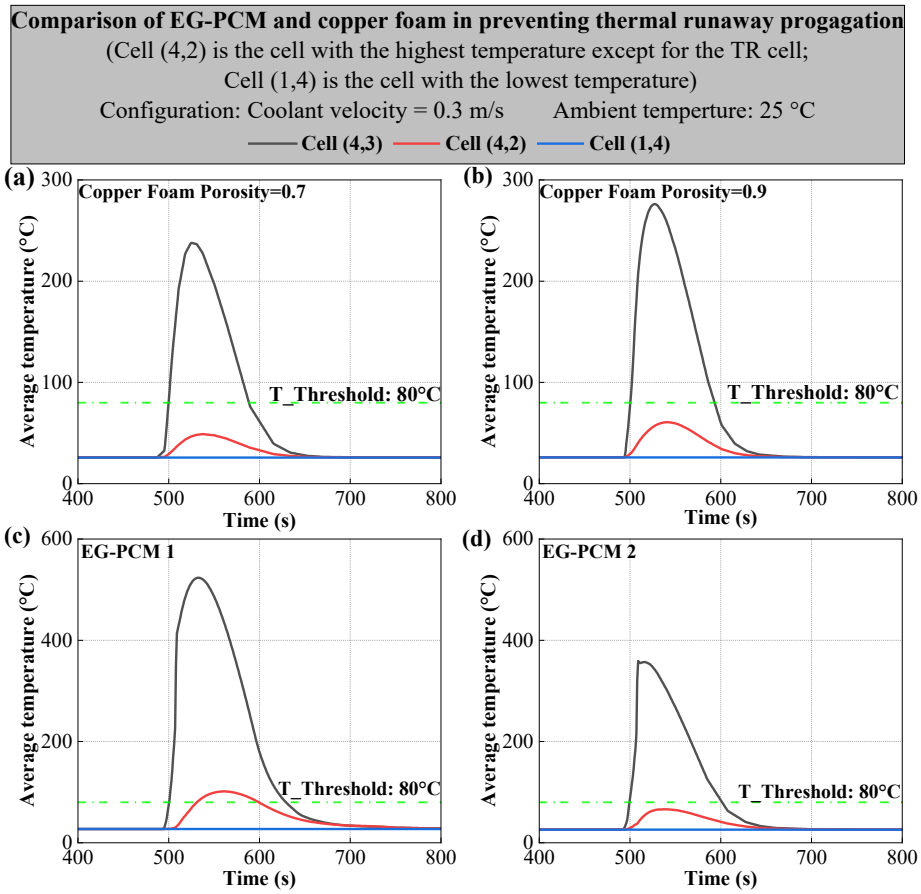

Fig. 6. Average cell temperature of three selected batteries during the single-cell TR event for the novel hybrid active-passive BTMS: (a) copper foam with a porosity of 0.7; (b) copper foam with a porosity of 0.9; (c) EG-PCM 1; (d) EG-PCM 2

It is crucial to examine the effect of coolant velocities on the prevention of TR propagation, as illustrated in Fig. 7. The flow rate of 0.01 m/s represents a near 'zero flow' case. The temperature of Cell (4,2) was reduced when the coolant velocity was increased from 0.01 m/s to 0.1 m/s; however, this effect diminished as the flow rate was increased from 0.1 m/s to 0.3 m/s. For copper foams with porosities of 0.7 and 0.9, the coolant flow required to prevent TR propagation was 0.10 m/s and 0.17 m/s, respectively. Similarly, the required flow rate for EG-PCM 2 is approximately 0.10 m/s. Cell (4,2) cannot be kept from TR with EG-PCM 1, at least not with the laminar coolant flow. As illustrated in Fig. 8, the cooling efficiency of the novel hybrid active-passive BTMS coupled with copper foam is influenced by porosity and coolant velocity. A coolant flow of 0.12 m/s to 0.15 m/s is required to achieve

the target of TR propagation prevention, depending on the copper porosity. Heat transfer of the active liquid cooling includes heat conduction and heat convection. The increase in coolant flow rate can effectively improve the convective heat transfer and significantly reduce the average temperature of the battery. In the case of PCM, thermal diffusion will be more through the coolant due to the low thermal conductivity of PCM. The increase in coolant flow rate may cause a faster heat transfer from the TR cell to the adjacent cells. Therefore, the maximum temperature in the adjacent cell of the TR cell with the coolant flow rate of 0.3 m/s has an extremely slight increase compared to the coolant flow rate of 0.2 m/s.

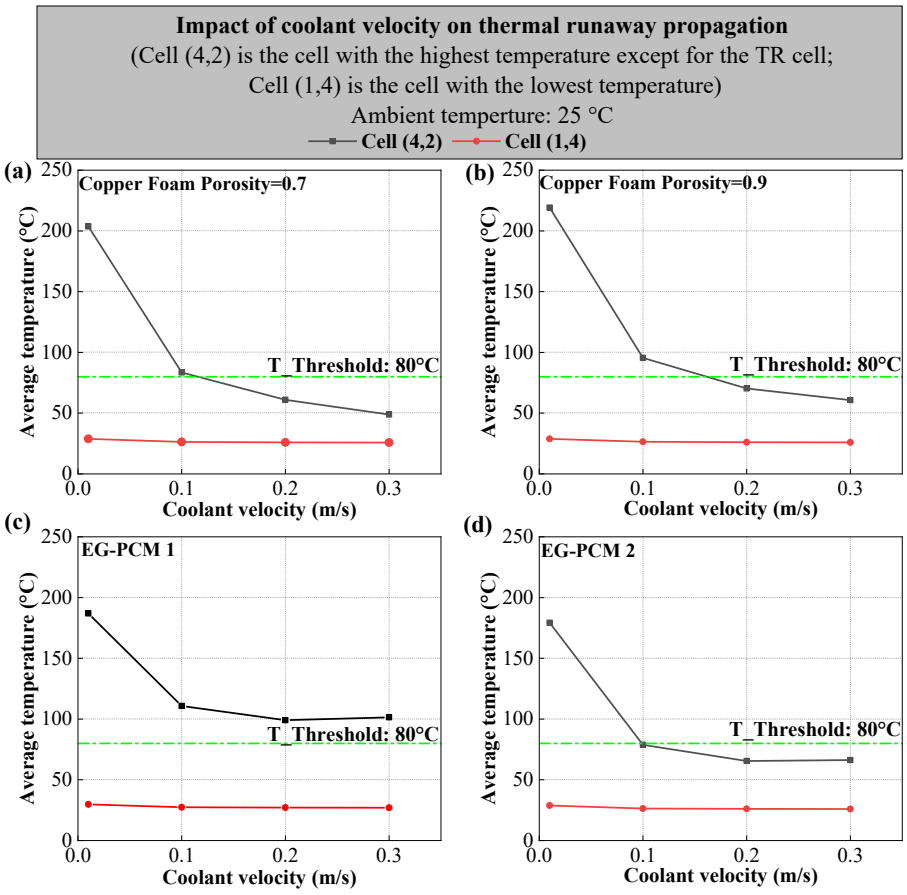

Fig. 7. Impact of coolant velocity on average cell temperature of cells during the single-cell TR event for the novel hybrid active-passive BTMS: (a) copper foam with a porosity of 0.7; (b) copper foam with a porosity of 0.9; (c) EG-PCM 1; (d) EG-PCM 2

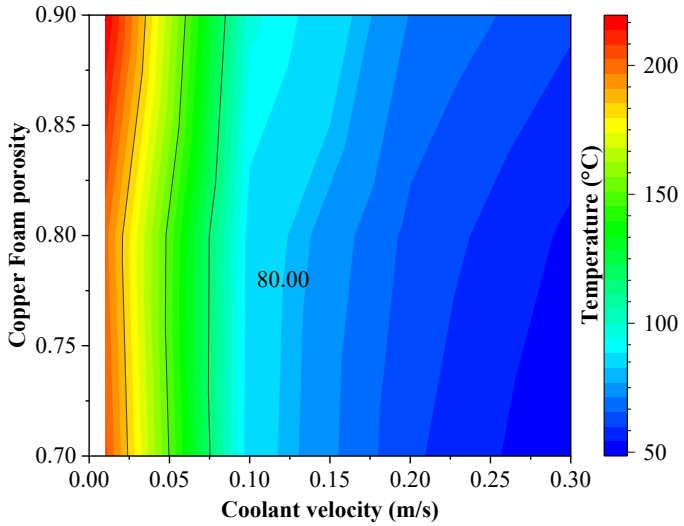

Fig. 8. Maximum temperature of Cell (4,2) under various liquid flow velocities and copper foam porosities during single-cell triggered TR.

4.2 Effects of cooling methods on the thermal behavior of battery under driving cycle

The primary function of the BTMS is to keep the temperature of the battery modules/packs within a narrow range (15-40 °C). As such, it is critical to assess its performance under typical battery operating conditions. Herein, battery thermal behaviors under an NEDC dynamic load were investigated. The average temperature variation of the battery module at a coolant velocity of 0 m/s-0.3 m/s is depicted in Fig. 9. Copper foam with high thermal diffusivity can rapidly dissipate the heat generated by the battery cells. PCM can absorb massive heat, benefiting from its high latent heat. The findings showed all cases examined, the average temperature and temperature differential of the battery module was kept below 30 °C and 0.2 °C, respectively. Under the NEDC load cycle, the battery module employing passive cooling can effectively eliminate the parasitic power consumption caused by active liquid cooling, thereby reducing the cost and size of BTMS.

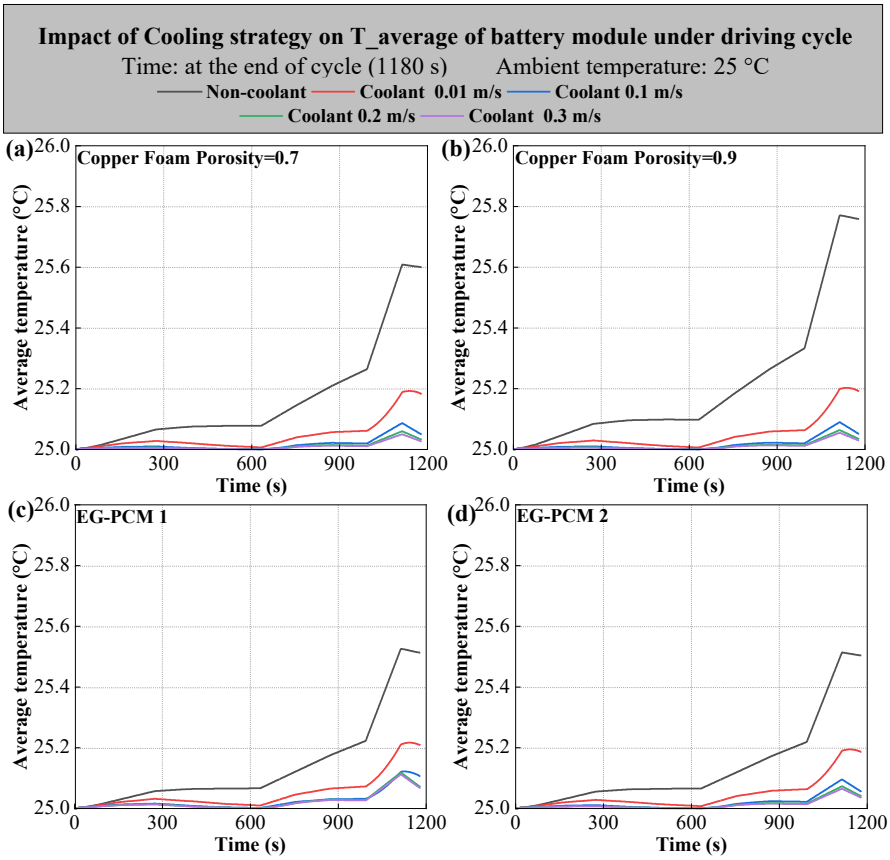

Fig. 9. Temperature of the battery module with coolant velocity from 0m/s to 0.3 m/s under NEDC: (a) copper foam with a porosity of 0.7; (b) copper foam with a porosity of 0.9; (c) EG-PCM 1; (d) EG-PCM 2

Fig. 10 shows the maximum temperature difference among cells at the coolant velocity of 0 - 0.3 m/s under the NEDC dynamic driving cycle. In the no-coolant cooling case, the temperature uniformity between cells is sufficient under driving cycle conditions. The maximum temperature difference between the battery cells is limited within 0.2 °C. The maximum temperature difference (ΔT) is defined by the difference between the highest temperature cell ($\bar{T}_{max}$) and the lowest temperature cell ($\bar{T}_{min}$) in the module:

$$\Delta T = \bar{T}_{max} - \bar{T}_{min} \tag{13}$$

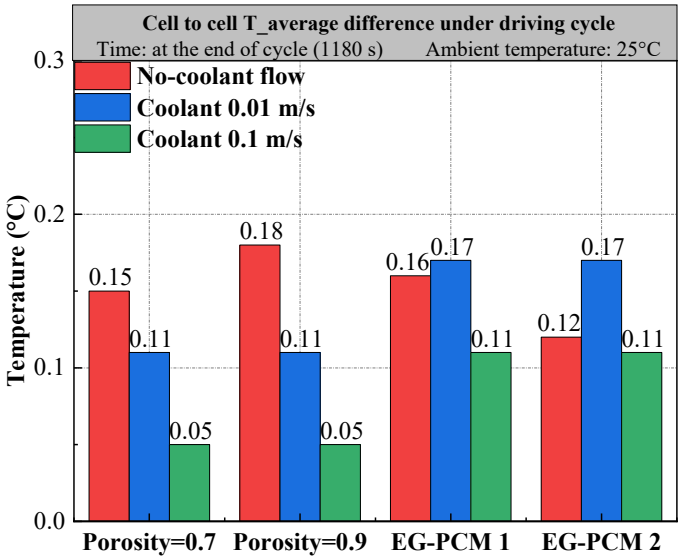

Fig. 10. Maximum cell-to-cell temperature difference in the module using various cooling strategies under NEDC.

4.3 Effects of cooling methods on the thermal behavior of battery under 3C-rate

Fig. 11 depicts the average temperature of the battery module during the 3 C constant charge/discharge cycle. The copper foam maintained a uniform temperature distribution effectively. When the module temperature reaches the phase transition temperature range, PCM with a high latent heat absorbs heat to maintain the module temperature within the phase transition temperature range. With EG-PCM, the maximum temperature of the cell can be limited to near the phase transition temperature, which is lower than with copper foam. However, once the battery temperature rises above the PCM phase transition temperature, the non-uniformity of the temperature of cells in the module is enlarged. Fig. 12 exhibits the average temperature of the module and temperature of selected cells with the novel hybrid BTMS. Active liquid cooling effectively reduces the temperature rise of the battery module. Except for LC-EG-PCM 1, the maximum temperature of the battery module was less than 27 °C. In comparison to EG-PCM, liquid cooling has a greater impact on copper foam. Compared with pure passive cooling, the average temperature of the battery module with copper foam porosity of 0.9

and EG-PCM 2 decreased by 72.5% and 52.7% at the coolant flow rate of 0.3 m/s. A copper foam with a lower porosity can improve the cooling performance. However, this advantage comes at the cost of a greater copper foam mass.

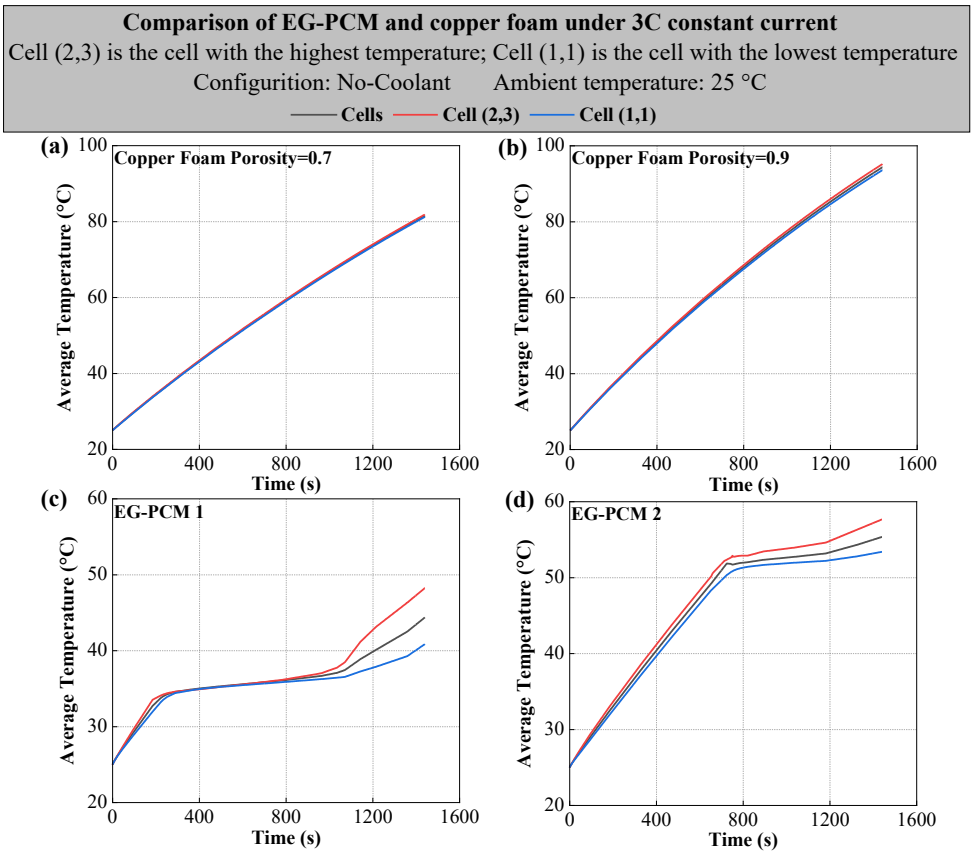

Fig. 11. The temperature variation of the battery module and selected cells using BTMS without coolant cooling under various cooling methods: (a) copper foam with a porosity of 0.7; (b) copper foam with a porosity of 0.9; (c) EG-PCM 1; (d) EG-PCM 2

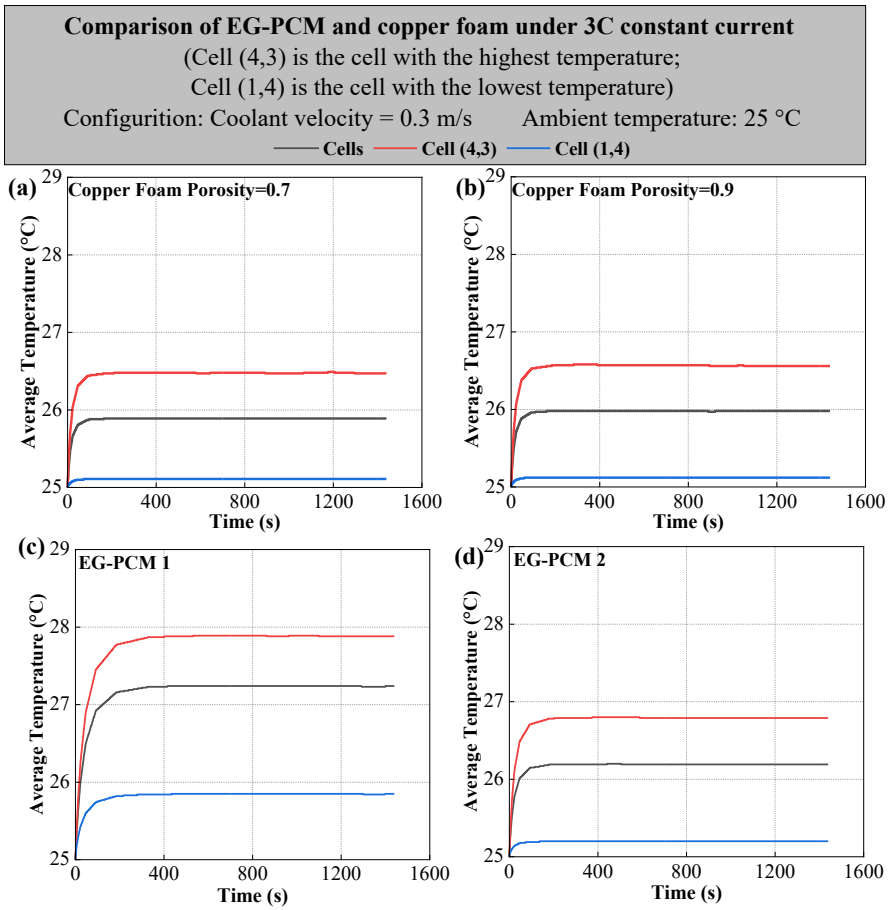

Fig. 12. Average temperature of the battery module and selected cells (a) copper foam with a porosity of 0.7; (b) copper foam with a porosity of 0.9; (c) EG-PCM 1; (d) EG-PCM 2

Fig. 13 depicts the average temperature of the module with varying porosity and coolant velocity. The temperature rise of the battery module is inversely correlated to the flow rate. The temperature of the battery module fluctuates only slightly between 25.9 °C and 30.8 °C when the porosity and coolant velocity is varied. Fig. 14 illustrates the average temperature difference between cells in a module. With no coolant flow, the maximum temperature difference in the battery module using EG-PCM 1 and EG-PCM 2 reach 7.4 ℃ and 4.2 ℃, respectively. The maximum temperature difference between cells in the module using LC-EG-PCM 1 and LC-EG-PCM 2 was reduced to 2.0 ℃ and 1.6 ℃, respectively. The results revealed that copper foam can effectively enhance the uniformity of temperature distribution

in the battery module due to its high thermal conductivity. The maximum temperature difference in the battery module with LC-CF is only 1.4 °C.

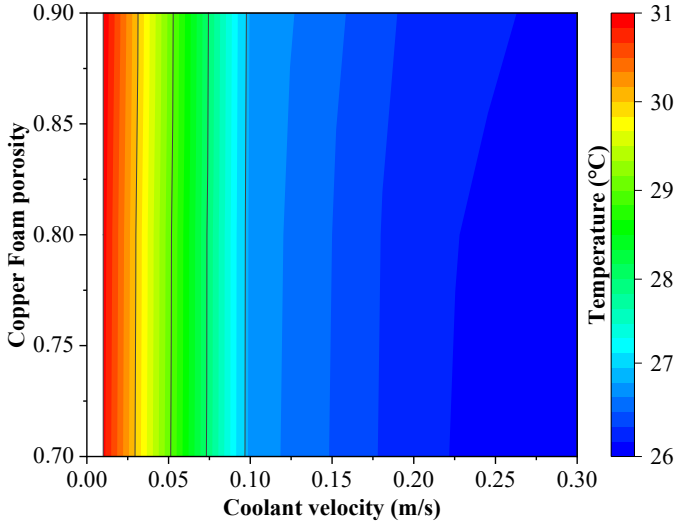

Fig. 13. Average temperature of battery module at different porosity and coolant velocity

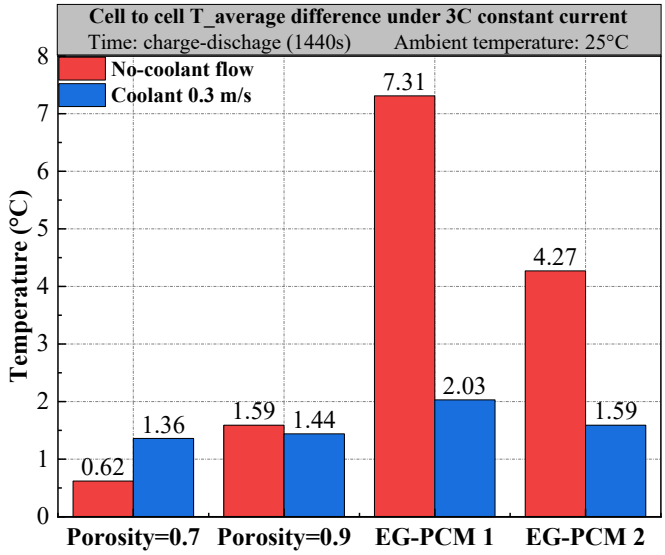

Fig. 14. Maximum cell-to-cell temperature difference in the module under 3 C constant current

5. Conclusion

In this study, a numerical analysis was conducted into the inhibiting effects of a novel hybrid BTMS combining active and passive cooling on TR propagation caused by single cell. EG-PCM and copper foam as passive cooling materials are independently utilized for thermal management.

Additionally, the effects of coolant flow rates and material on the temperature rise and temperature uniformity of the battery module were studied under a load of NEDC driving cycle and 3C discharge rates. The conclusions drawn from the study can be summarized as follows:

1) Thermal runaway propagation in the battery module can be effectively prevented by incorporating active liquid cooling and passive cooling. The hybrid BTMS using copper foam with porosity of 0.7 and EG-PCM with a melting temperature of 52°C and thermal diffusivity of 9.68 mm^2/s can limit the maximum temperature of the battery cell (except TR cell) to 48.9°C and 66.2°C, respectively, which were below the safety threshold (80 °C).

2) Porosity determines the heat dissipation performance of the copper foam in the proposed hybrid BTMS. The maximum cell temperature (except for the TR cell) can be reduced from 60.7 °C to 48.9 °C (-19.4 %) if the porosity of copper foam is changing from 0.9 to 0.7.

3) The numerical analysis results showed that under the NEDC driving cycle, PCM or copper foam can effectively maintain temperature uniformity and temperature rise within the optimal range.

4) Active liquid cooling can transmit the heat stored in passive cooling materials and enhance the heat dissipation capacity of BTMS. The average temperature of the battery module with active cooling can be up to 72% lower than the battery module without active liquid cooling under the 3C discharge rate.

6. Limitations and future research

This study has some limitations in experimental verification and optimization of thermal management systems. In future research, the authors will experimentally investigate the thermal runaway propagation process and the thermal behavior of battery modules under various active/passive

cooling strategies. Based on finite element analysis, the optimization works of the battery thermal management system in parasitic power consumption, volume, and heat dissipation will also be conducted.

Appendix

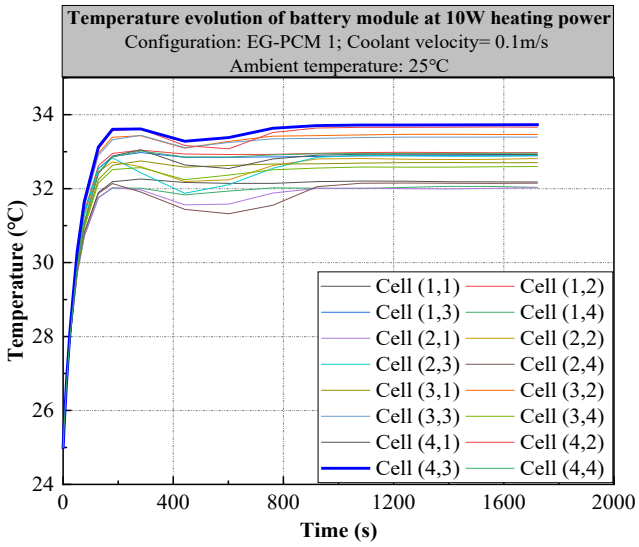

Fig. 1A. Average temperature of battery module with hybrid active-passive BTMS at a 10 heat generation rate

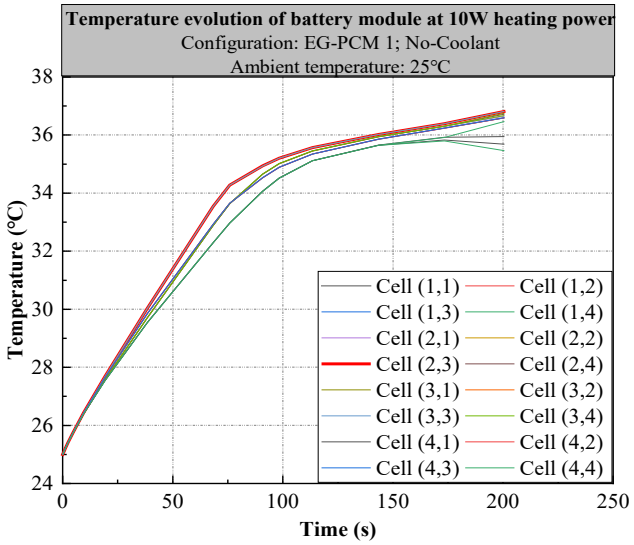

Fig. 2A. Average temperature of battery module with passive BTMS at a 10 heat generation rate

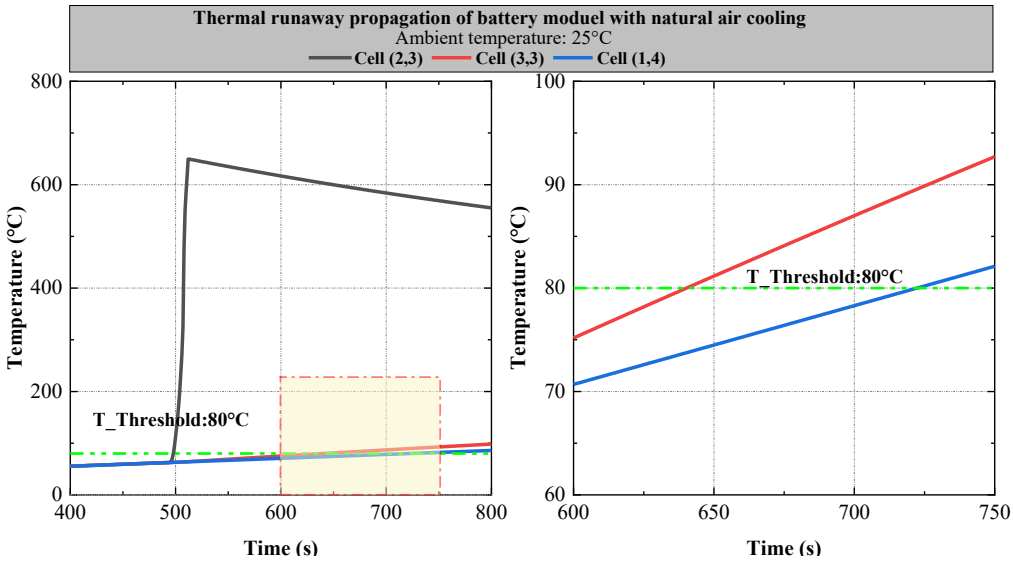

Fig. 3A. Average cell temperature of three selected batteries during the single-cell TR event for BTMS with natural air cooling

References

[1] Y.S. Duh, J.H. Theng, C.C. Chen, C.S. Kao, Comparative study on thermal runaway of commercial 14500, 18650 and 26650 LiFePO4 batteries used in electric vehicles, J. Energy Storage. 31 (2020) 101580. https://doi.org/10.1016/j.est.2020.101580.

[2] J. Zhang, L. Zhang, F. Sun, Z. Wang, An Overview on Thermal Safety Issues of Lithium-ion Batteries for Electric Vehicle Application, IEEE Access. 6 (2018) 23848–23863. https://doi.org/10.1109/ACCESS.2018.2824838.

[3] J. Kim, J. Oh, H. Lee, Review on battery thermal management system for electric vehicles, Appl. Therm. Eng. 149 (2019) 192–212. https://doi.org/10.1016/j.applthermaleng.2018.12.020.

[4] X. Feng, M. Ouyang, X. Liu, L. Lu, Y. Xia, X. He, Thermal runaway mechanism of lithium ion battery for electric vehicles: A review, Energy Storage Mater. 10 (2018) 246–267. https://doi.org/10.1016/j.ensm.2017.05.013.

[5] D. Ren, X. Feng, L. Liu, H. Hsu, L. Lu, L. Wang, X. He, M. Ouyang, Investigating the relationship between internal short circuit and thermal runaway of lithium-ion batteries under thermal abuse condition, Energy Storage Mater. 34 (2021) 563–573. https://doi.org/10.1016/j.ensm.2020.10.020.

[6] C. Yuan, Q. Wang, Y. Wang, Y. Zhao, Inhibition effect of different interstitial materials on thermal runaway propagation in the cylindrical lithium-ion battery module, Appl. Therm. Eng. 153 (2019) 39–50. https://doi.org/10.1016/j.applthermaleng.2019.02.127.

[7] X. Feng, X. He, M. Ouyang, L. Lu, P. Wu, C. Kulp, S. Prasser, Thermal runaway propagation model for designing a safer battery pack with 25Ah LiNixCoyMnzO2 large format lithium ion battery, Appl. Energy. 154 (2015) 74–91. https://doi.org/10.1016/j.apenergy.2015.04.118.

[8] T. Yamada, T. Koshiyama, M. Yoshikawa, T. Yamada, N. Ono, Analysis of a lithium-ion battery cooling system for electric vehicles using a phase-change material and heat pipes, J. Therm. Sci. Technol. 12 (2017) 1–15. https://doi.org/10.1299/jtst.2017jtst0011.

[9] C. Jin, Y. Sun, H. Wang, Y. Zheng, S. Wang, X. Rui, C. Xu, X. Feng, H. Wang, M. Ouyang, Heating power and heating energy effect on the thermal runaway propagation characteristics of lithium-ion battery module: Experiments and modeling, Appl. Energy. 312 (2022) 118760. https://doi.org/10.1016/j.apenergy.2022.118760.

[10] P. Jindal, B.S. Kumar, J. Bhattacharya, Coupled electrochemical-abuse-heat-transfer model to predict thermal runaway propagation and mitigation strategy for an EV battery module, J. Energy Storage. 39 (2021) 102619. https://doi.org/10.1016/j.est.2021.102619.

[11] M. Suresh Patil, J.H. Seo, M.Y. Lee, A novel dielectric fluid immersion cooling technology for Li-ion battery thermal management, Energy Convers. Manag. 229 (2021) 113715. https://doi.org/10.1016/j.enconman.2020.113715.

[12] P. Huang, C. Yao, B. Mao, Q. Wang, J. Sun, Z. Bai, The critical characteristics and transition process of lithium-ion battery thermal runaway, Energy. 213 (2020) 119082. https://doi.org/10.1016/j.energy.2020.119082.

[13] P. Dubey, G. Pulugundla, A.K. Srouji, Direct comparison of immersion and cold-plate based cooling for automotive li-ion battery modules, Energies. 14 (2021). https://doi.org/10.3390/en14051259.

[14] K. Smith, C.Y. Wang, Power and thermal characterization of a lithium-ion battery pack for hybrid-electric vehicles, J. Power Sources. 160 (2006) 662–673. https://doi.org/10.1016/j.jpowsour.2006.01.038.

[15] S. Abada, G. Marlair, A. Lecocq, M. Petit, V. Sauvant-moynot, F. Huet, Safety focused modeling of lithium-ion batteries : A review, J. Power Sources. 306 (2016) 178–192. https://doi.org/10.1016/j.jpowsour.2015.11.100.

[16] K. Darcovich, D.D. MacNeil, S. Recoskie, B. Kenney, Coupled electrochemical and thermal battery models for thermal management of prismatic automotive cells, Appl. Therm. Eng. 133 (2018) 566–575. https://doi.org/10.1016/j.applthermaleng.2018.01.094.

[17] D. Chen, J. Jiang, G.H. Kim, C. Yang, A. Pesaran, Comparison of different cooling methods for lithium ion battery cells, Appl. Therm. Eng. 94 (2016) 846–854. https://doi.org/10.1016/j.applthermaleng.2015.10.015.

[18] X. Feng, D. Ren, X. He, M. Ouyang, Mitigating Thermal Runaway of Lithium-Ion Batteries, Joule. 4 (2020) 743–770. https://doi.org/10.1016/j.joule.2020.02.010.

[19] K. Li, J. Yan, H. Chen, Q. Wang, Water cooling based strategy for lithium ion battery pack dynamic cycling for thermal management system, Appl. Therm. Eng. 132 (2018) 575–585. https://doi.org/10.1016/j.applthermaleng.2017.12.131.

[20] J. Weng, C. Xiao, D. Ouyang, X. Yang, M. Chen, G. Zhang, R.K.K. Yuen, J. Wang, Mitigation effects on thermal runaway propagation of structure-enhanced phase change material modules with flame retardant additives, Energy. 239 (2022) 122087. https://doi.org/10.1016/j.energy.2021.122087.

[21] M. Yang, H. Wang, W. Shuai, X. Deng, Thermal optimization of a kirigami-patterned wearable lithium-ion battery based on a novel design of composite phase change material, Appl. Therm. Eng. 161 (2019) 114141. https://doi.org/10.1016/j.applthermaleng.2019.114141.

[22] L.H. Saw, Y. Ye, M.C. Yew, W.T. Chong, M.K. Yew, T.C. Ng, Computational fluid dynamics simulation on open cell aluminium foams for Li-ion battery cooling system, Appl. Energy. 204 (2017) 1489–1499. https://doi.org/10.1016/j.apenergy.2017.04.022.

[23] F. Chen, R. Huang, C. Wang, X. Yu, H. Liu, Q. Wu, K. Qian, R. Bhagat, Air and PCM cooling for battery thermal management considering battery cycle life, Appl. Therm. Eng. 173 (2020) 115154. https://doi.org/10.1016/j.applthermaleng.2020.115154.

[24] A. Vadakkepatt, B. Trembacki, S.R. Mathur, J.Y. Murthy, Bruggeman's Exponents for Effective Thermal Conductivity of Lithium-Ion Battery Electrodes, J. Electrochem. Soc. 163 (2016) A119–A130. https://doi.org/10.1149/2.0151602jes.

[25] S.K. Mohammadian, S.M. Rassoulinejad-Mousavi, Y. Zhang, Thermal management improvement of an air-cooled high-power lithium-ion battery by embedding metal foam, J. Power Sources. 296 (2015) 305–313. https://doi.org/10.1016/j.jpowsour.2015.07.056.

[26] Samsung, Specification of product INR18650-20R, (2011) 0–15. http://www.datasheet-pdf.com/datasheet/Samsung/799163/INR18650-20R.pdf.html.

[27] K.F. Amin, H.M.M.A. Rashed, Steel Used in Construction Industries, Ref. Modul. Mater. Sci. Mater. Eng. (2019). https://doi.org/10.1016/b978-0-12-803581-8.10270-x.

[28] R. Sabbah, R. Kizilel, J.R. Selman, S. Al-Hallaj, Active (air-cooled) vs. passive (phase change material) thermal management of high power lithium-ion packs: Limitation of temperature rise and uniformity of temperature distribution, J. Power Sources. 182 (2008) 630–638. https://doi.org/10.1016/j.jpowsour.2008.03.082.

[29] Y. Zhao, Q. Li, B. Zou, T. Zhang, L. Jin, G. Qiao, B. Nie, Y. Huang, Y. Ding, Performance of a liquid cooling-based battery thermal management system with a composite phase change material, Int. J. Energy Res. 44 (2020) 4727–4742. https://doi.org/10.1002/er.5254.

[30] R.H. Plante, Chapter three - Determining Energy Usage, in: R.H. Plante (Ed.), Sol. Energy, Photovoltaics, Domest. Hot Water.., Academic Press, Boston, 2014: pp. 27–39. https://doi.org/https://doi.org/10.1016/B978-0-12-420155-2.00003-7.

[31] Z. Sun, R. Fan, F. Yan, T. Zhou, N. Zheng, Thermal management of the lithium-ion battery by the composite PCM-Fin structures, Int. J. Heat Mass Transf. 145 (2019) 118739. https://doi.org/https://doi.org/10.1016/j.ijheatmasstransfer.2019.118739.

[32] B. Xia, B. Ye, J. Cao, Polarization Voltage Characterization of Lithium-Ion Batteries Based on a Lumped Diffusion Model and Joint Parameter Estimation Algorithm, Energies. 15 (2022). https://doi.org/10.3390/en15031150.